A Letters Journal Exploring the Frontiers of Physics

June 2023

EPL, **142** (2023) 67001 www.epljournal.org
doi: 10.1209/0295-5075/acd8e9

**Focus Article**

# Taxis of cargo-carrying microswimmers in traveling activity waves[(a)]

Pietro Luigi Muzzeddu[1], Édgar Roldán[2], Andrea Gambassi[1,3] and Abhinav Sharma[4,5(b)]

[1] *SISSA, International School for Advanced Studies - via Bonomea 265, 34136 Trieste, Italy*
[2] *ICTP, The Abdus Salam International Centre for Theoretical Physics - Strada Costiera 11, 34151 Trieste, Italy*
[3] *INFN, Sezione di Trieste - Trieste, Italy*
[4] *Faculty of Mathematics, Natural Sciences, and Materials Engineering: Institute of Physics, University of Augsburg Universitätsstraße 1, 86159 Augsburg, Germany*
[5] *Leibniz-Institut für Polymerforschung Dresden, Institut Theorie der Polymere - 01069 Dresden, Germany*

received 17 February 2023; accepted in final form 25 May 2023
published online 6 June 2023

**Abstract** – Many fascinating properties of biological active matter crucially depend on the capacity of constituting entities to perform directed motion, *e.g.*, molecular motors transporting vesicles inside cells or bacteria searching for food. While much effort has been devoted to mimicking biological functions in synthetic systems, such as transporting a cargo to a targeted zone, theoretical studies have primarily focused on single active particles subject to various spatial and temporal stimuli. Here we study the behavior of a self-propelled particle carrying a passive cargo in a travelling activity wave and show that this active-passive dimer displays a rich, emergent tactic behavior. For cargoes with low mobility, the dimer always drifts in the direction of the wave propagation. For highly mobile cargoes, instead, the dimer can also drift against the traveling wave. The transition between these two tactic behaviors is controlled by the ratio between the frictions of the cargo and the microswimmer. In slow activity waves the dimer can perform an *active surfing* of the wave maxima, with an average drift velocity equal to the wave speed. These analytical predictions, which we confirm by numerical simulations, might be useful for the future efficient design of bio-hybrid microswimmers.



**Introduction.** – The ability to self-propel at the expense of fuel consumption is a fundamental property of active matter [1–4]. In the biological context, self-propelling microscopic systems perform functions that require accurate directed transport, for instance, white blood cells chase intruders [5], motor proteins transport RNA inside cells [6] and microswimmers such as *E. coli* [7] and sperm cells [8] steer themselves towards sources of nutrients. Directed transport is a highly desirable property, in particular for applications in drug delivery at the nanoscale [9–13]. For this purpose, bio-hybrid microswimmers have been designed by integrating biological entities with synthetic constructs, *e.g.*, bacteria capable to transport and drop off passive microscopic cargo to specific target locations [14–17].

Bacteria and eukaryotic cells [18,19] generally navigate in dynamic activating media and react *in vivo* to time-dependent tactic stimuli of various nature. Such an interaction with travelling activity signals, *e.g.*, chemical waves [20,21], leads to fascinating collective behavior [22] and sometimes to unexpected migration phenomena, as in the case of the so-called *chemotactic wave paradox* [20,23]. While synthetic active particles mimic the basic features of self-propulsion and persistence of actual biological active matter, they lack the information processing capacity and motoric control which is essential for directed transport in biological and bio-hybrid systems. Despite their memory-less response to tactic signals, artificial self-propelled particles exhibit directed transport when

[(a)] Contribution to the Focus Issue *Statistical Physics of Self-Propelled Colloids* edited by Hartmut Löwen, Sabine Klapp and Holger Stark.

[(b)] E-mail: abhinav.sharma@physik.uni-augsburg.de (corresponding author)

immersed in travelling waves controlling locally their degree of activity (*e.g.*, their self-propulsion velocity), as shown experimentally with phototactic Janus particles exposed to propagating optical pulses [24]. Several theoretical studies have focused on controlling and directing the motion of a single self-propelled particle in a fluctuating environment [25–29]. However, a fundamental understanding of the behavior of cargo-carrying microswimmers in time-dependent activity is still lacking.

It has been already shown that chemically active colloidal particles can be employed as carriers of catalytically inert cargoes at the micro-scale [30,31]. Cargo-carrying self-propelled particles have also been analyzed in stationary and spatially inhomogeneous activity fields [32]. While a single self-propelled particle always accumulates in regions with low activity, attaching a passive cargo reverses this tendency. In fact, beyond a certain threshold cargo, the particle accumulates in regions with larger activity [32]. While preferential accumulation could be regarded as a signature of the tactic behavior [32], in the case of stationary activity, it causes no transport of the dimer. By contrast, for a time-dependent activity, such as a source emitting activity pulses, the tactic behavior of an active particle can result in motion towards or away from the source. With this motivation, in this paper we study active-passive dimers subject to a time-dependent activity in the form of a travelling wave. We analytically show that the dimer exhibits directed transport, characterized by a wave-induced drift. The direction of this drift depends on the wave speed, being opposite to its propagation direction for a slow wave but along it for a fast wave. Interestingly, the opposite drift vanishes at a threshold cargo upon increasing its friction, beyond which the dimer only shows drift along the propagation direction. Our theoretical treatment of the active-passive dimer is based on the active Ornstein-Uhlenbeck particle (AOUP) model of activity [33–36]. Furthermore, our analysis shows that the tactic behavior of a cargo-carrying AOUPs is equivalent to that of a similar active-passive dimeric complex where the active unit is modeled as an active Brownian particle (ABP) [32].

**The model.** – In this section we introduce a minimal model for the dynamics of an active microswimmer dragging a passive load in $d$ spatial dimensions within an inhomogeneous and time-dependent environment. The microswimmer at position $\boldsymbol{r}$ and time $t$ interacts with a tactic signal described by the activity field $v_{\rm a}(\boldsymbol{r}-\boldsymbol{v}_w t)$, which propagates with velocity $\boldsymbol{v}_w = v_w \boldsymbol{e}_0$ along the direction of the unit vector $\boldsymbol{e}_0$, as depicted in fig. 1. The shape of the traveling wave $v_{\rm a}(\boldsymbol{r}-\boldsymbol{v}_w t)$ will remain generic unless specified otherwise. As usually done for $\mu$m-sized colloidal particles in a liquid, we assume that viscous forces dominate over inertial effects and therefore we consider an overdamped dynamics for the active-passive dimer, which


Fig. 1: Sketch of the stochastic model described by eqs. (1) in two spatial dimensions. A self-propelled active microswimmer (blue ellipse) in a fluid drags a passive cargo (gray circle) via a harmonic interaction (blue spring). The instantaneous self-propulsion velocity of the microswimmer (blue arrow) is locally controlled by a sinusoidal traveling wave of activity, which propagates through the fluid with phase velocity $v_w$ along the unit vector $\boldsymbol{e}_0$. For illustration we sketch here two examples of active-passive dimers, one with a low-friction cargo ($q$ small, left) and the other with a high-friction cargo ($q$ large, right).

is governed by the following Langevin equations:

$$\dot{\boldsymbol{r}}_1 = -\frac{1}{\gamma}\nabla_{\boldsymbol{r}_1} U(\boldsymbol{r}_1-\boldsymbol{r}_2) + v_{\rm a}(\boldsymbol{r}_1-\boldsymbol{v}_w t)\boldsymbol{\eta} + \sqrt{2D}\boldsymbol{\xi}_1, \quad \text{(1a)}$$

$$\dot{\boldsymbol{r}}_2 = -\frac{1}{q\gamma}\nabla_{\boldsymbol{r}_2} U(\boldsymbol{r}_1-\boldsymbol{r}_2) + \sqrt{\frac{2D}{q}}\boldsymbol{\xi}_2, \quad \text{(1b)}$$

$$\tau\dot{\boldsymbol{\eta}} = -\boldsymbol{\eta} + \sqrt{\frac{2\tau}{d}}\boldsymbol{\xi}_3, \quad \text{(1c)}$$

where $\boldsymbol{r}_1$ and $\boldsymbol{r}_2$ denote the positions of the active microswimmer and the passive cargo, respectively. The interaction $U(\boldsymbol{r}_1-\boldsymbol{r}_2)$ between them is modeled by an isotropic parabolic potential $U(\boldsymbol{r}) = \kappa\boldsymbol{r}^2/2$, with stiffness $\kappa > 0$ and zero rest length. The stochastic forces $\boldsymbol{\xi}_1$, $\boldsymbol{\xi}_2$, $\boldsymbol{\xi}_3$ are three independent zero-mean Gaussian white noises accounting for thermal fluctuations. Moreover, the active carrier exploits local energy injections to self-propel along the direction of the propulsion vector $\boldsymbol{\eta}$ which is given by a set of $d$ independent Ornstein-Uhlenbeck processes with variance $1/d$ and correlation time $\tau$. It follows that $\boldsymbol{\eta}$ is a zero-mean Gaussian colored noise with autocorrelation function $\langle \eta_\alpha(t)\eta_\beta(s)\rangle = (\delta_{\alpha,\beta}/d)\exp(-|t-s|/\tau)$, where $\delta_{\alpha,\beta}$ denotes Kronecker's delta. This normalization ensures that the average modulus squared of the propulsion vector is $\langle \|\boldsymbol{\eta}\|^2\rangle = 1$ for all values of $d$. While the time scale $\tau$ sets the persistence of the self-propulsion force, its strength is modulated in space by the activity field $v_{\rm a}$. Note that, in this minimal model, the rotational dynamics of the active carrier is not affected by the interaction potential between the two monomers and there is no coupling between the dimer main axis and the polarity of the active particle. In order to recover an equilibrium dynamics in the absence of activity $v_{\rm a} = 0$, we connect the mobility $\gamma^{-1}$ and the diffusivity $D$ via the Einstein relation $D = k_{\rm B}T/\gamma$. Moreover, the cargo and the active carrier are assumed to have different friction coefficients, the ratio of which is given by the parameter $q$. In a Newtonian fluid and for spherical colloidal carrier and cargo, $q$ equals the ratio of the radius of the cargo to that of the carrier.

The Langevin dynamics in eqs. (1) can be more conveniently written in terms of the dimer position in the

comoving frame, which we identify with the centre of friction $\boldsymbol{\chi} = (\boldsymbol{r}_1 + q\boldsymbol{r}_2)/(1+q) - \boldsymbol{v}_w t$ and the distance $\boldsymbol{r} = \boldsymbol{r}_1 - \boldsymbol{r}_2$. Changing variables $(\boldsymbol{r}_1, \boldsymbol{r}_2, \boldsymbol{\eta}) \to (\boldsymbol{\chi}, \boldsymbol{r}, \boldsymbol{\eta})$ to the new coordinate system, the Fokker-Planck equation for the probability density $P(\boldsymbol{\chi}, \boldsymbol{r}, \boldsymbol{\eta}, t)$ associated to the stochastic dynamics in eqs. (1) reads

$$\begin{aligned}\partial_t P(\boldsymbol{\chi}, \boldsymbol{r}, \boldsymbol{\eta}, t) &= \frac{1}{d\tau}\hat{\mathcal{L}}_{\boldsymbol{\eta}} P \\ &- \nabla_{\boldsymbol{\chi}} \cdot \left[ -\boldsymbol{v}_w P + \frac{1}{1+q} v_{\mathrm{a}}(\boldsymbol{\chi}')\, \boldsymbol{\eta} P - \frac{D}{1+q}\nabla_{\boldsymbol{\chi}} P \right] \\ &- \nabla_{\boldsymbol{r}} \cdot \left[ -\frac{1+q}{q\gamma}\nabla_{\boldsymbol{r}} U P + v_{\mathrm{a}}(\boldsymbol{\chi}')\, \boldsymbol{\eta} P - \frac{1+q}{q} D \nabla_{\boldsymbol{r}} P \right],\end{aligned} \tag{2}$$

with $\boldsymbol{\chi}' = \boldsymbol{\chi} + q\boldsymbol{r}/(1+q)$ and $\hat{\mathcal{L}}_{\boldsymbol{\eta}} P = \nabla^2_{\boldsymbol{\eta}} P + d\nabla_{\boldsymbol{\eta}} \cdot (\boldsymbol{\eta} P)$.

**Transport properties for slow activity waves.** – In order to estimate the extent to which the propagating tactic signal affects the directed motion of the cargo-carrying microswimmer, we focus on transport properties induced by the activity travelling wave. Starting from eq. (2), we derive in the Supplementary Material `Supplementarymaterial.pdf` (SM) an effective mean-field dynamics which describes the evolution of the system at time scales longer than $\tau$ and length scales larger than the typical persistence length $l_p \sim \langle v_{\mathrm{a}} \rangle \tau$ analogously to ref. [37]. This provides a generalised hydrodynamics for the relevant fields such as particle density, polarization, etc. In particular, the predictions deriving from it are expected to be valid for an activity which varies slowly on the length scale $l_p$ (*large wavelength* approximation). Importantly, we emphasize that our model ignores the hydrodynamic contributions arising from the interaction of the dimer with the surrounding solvent, thus falling into the class of dry active matter models [3]. In order to identify the fields with a relaxation time which grows indefinitely upon increasing the wavelength (*i.e.*, the slow modes), we perform a moment expansion analogous to, *e.g.*, refs. [37–39].

The evolution of the modes is described by a hierarchical structure, the detailed derivation of which is reported in sect. 1 of the SM. Importantly, we note that the zeroth order mode $\varphi(\boldsymbol{\chi}, \boldsymbol{r}, t) = \int \mathrm{d}\boldsymbol{\eta}\, P(\boldsymbol{\chi}, \boldsymbol{r}, \boldsymbol{\eta}, t)$, which describes the density related to the spatial marginal variables $\boldsymbol{\chi}$ and $\boldsymbol{r}$, is the only slow mode of the system. Indeed, $\varphi(\boldsymbol{\chi}, \boldsymbol{r}, t)$ is associated with a conservation law and its dynamics has the form of a continuity equation,

$$\begin{aligned}\partial_t \varphi(\boldsymbol{\chi}, \boldsymbol{r}, t) &= -\partial_\alpha \left[ -v_w \delta_{\alpha,0}\varphi + \frac{v_{\mathrm{a}}(\boldsymbol{\chi}')\,\sigma_\alpha}{(1+q)} - \frac{D}{1+q}\partial_\alpha \varphi \right] \\ &- \partial'_\alpha \left[ -\frac{(1+q)}{q\gamma}\partial'_\alpha U\varphi + v_{\mathrm{a}}(\boldsymbol{\chi}')\,\sigma_\alpha - \frac{(1+q)D}{q}\partial'_\alpha \varphi \right],\end{aligned} \tag{3}$$

where we introduced the shorthand notation $\partial_\alpha \equiv \partial_{\chi_\alpha}$ and $\partial'_\alpha \equiv \partial_{r_\alpha}$, while repeated indices imply summation. Furthermore, $\sigma_\alpha$ is the $\alpha$-th component of the first-order mode $\boldsymbol{\sigma}(\boldsymbol{\chi}, \boldsymbol{r}, t) = \int \mathrm{d}\boldsymbol{\eta}\, \boldsymbol{\eta} P(\boldsymbol{\chi}, \boldsymbol{r}, \boldsymbol{\eta}, t)$, which is related to the conditional average polarization at fixed spatial variables. Its dynamics is governed by

$$\begin{aligned}\partial_t \sigma_\alpha(\boldsymbol{\chi}, \boldsymbol{r}, t) = &-\frac{\partial_\alpha \left[ v_{\mathrm{a}}(\boldsymbol{\chi}')\,\varphi \right]}{(1+q)d} - \frac{\partial'_\alpha \left[ v_{\mathrm{a}}(\boldsymbol{\chi}')\,\varphi \right]}{d} \\ &+ \frac{(1+q)}{q\gamma}\partial'_\beta \left[ \partial'_\beta U \sigma_\alpha \right] - \tau^{-1}\sigma_\alpha + \mathcal{O}(\partial^2),\end{aligned} \tag{4}$$

where dependencies on higher-order modes are included in $\mathcal{O}(\partial^2)$. Notably, the decay rate due to the sink term $-\tau^{-1}\sigma_\alpha$ makes $\sigma_\alpha(\boldsymbol{\chi}, \boldsymbol{r}, t)$ a fast mode which does not obey a conservation law and which can be described by a quasi-static approximation. Moreover, the contribution $\mathcal{O}(\partial^2)$ of higher-order gradients is negligible under the assumption of a slowly varying activity field.

The combination of large-wavelength approximation and quasi-stationarity of $\boldsymbol{\sigma}(\boldsymbol{\chi}, \boldsymbol{r}, t)$ at time scales longer than $\tau$ provides a closure scheme for the hierarchy without needing information about higher-order modes. In particular, after integrating out the relative coordinate $\boldsymbol{r}$, we derive an effective drift-diffusion equation for the marginal density $\rho(\boldsymbol{\chi}, t) = \int \mathrm{d}\boldsymbol{r}\varphi(\boldsymbol{\chi}, \boldsymbol{r}, t)$ (see sect. 2 of the SM for the detailed derivation), which reads

$$\partial_t \rho(\boldsymbol{\chi}, t) = -\nabla_{\boldsymbol{\chi}} \cdot [\boldsymbol{V}_{\mathrm{eff}}(\boldsymbol{\chi})\rho(\boldsymbol{\chi}, t) - \nabla_{\boldsymbol{\chi}}(D_{\mathrm{eff}}(\boldsymbol{\chi})\rho(\boldsymbol{\chi}, t))], \tag{5}$$

where the effective drift and effective diffusivity are given, respectively, by

$$\boldsymbol{V}_{\mathrm{eff}}(\boldsymbol{\chi}) = (1 - \epsilon/2)\nabla_{\boldsymbol{\chi}} D_{\mathrm{eff}}(\boldsymbol{\chi}) - \boldsymbol{v}_w, \tag{6}$$

$$D_{\mathrm{eff}}(\boldsymbol{\chi}) = \frac{D}{1+q} + \frac{\tau v_{\mathrm{a}}^2(\boldsymbol{\chi})}{d(1+q)^2}. \tag{7}$$

This expression of $D_{\mathrm{eff}}$ reveals an enhancement of the diffusivity $D/(1+q)$ of the center of friction induced by the activity via a term $\propto v_{\mathrm{a}}^2(\boldsymbol{\chi})$.

Interestingly, the alignment of the effective drift with the activity gradient is controlled by the *tactic coupling*

$$\epsilon = 1 - \frac{q}{1 + \frac{1+q}{q}\frac{\tau}{\tau_{\mathrm{r}}}}, \tag{8}$$

where $\tau_{\mathrm{r}} = \gamma/\kappa$ is the characteristic spring relaxation time. The role of $\epsilon$ can be understood by considering the case of static activity field. In fact, for $v_w = 0$, the stationary density obtained from eq. (5) is

$$\rho(\boldsymbol{\chi}) = \mathcal{N}^{-1} \left[ 1 + \frac{\tau v_{\mathrm{a}}^2(\boldsymbol{\chi})}{dD(1+q)} \right]^{-\epsilon/2}. \tag{9}$$

Accordingly, $\epsilon$ determines the preferential accumulation of the dimer in the regions with high or low activity depending on its sign. Here, $\mathcal{N}$ is a normalization constant. Equation (8) implies that for a fixed $\tau/\tau_{\mathrm{r}}$, the tactic coupling $\epsilon$ is entirely determined by the friction ratio $q$, because it changes sign at the threshold value

$$q_{\mathrm{th}} = \frac{1}{2}\left[ 1 + \tau/\tau_{\mathrm{r}} + \sqrt{(1+\tau/\tau_{\mathrm{r}})^2 + 4\tau/\tau_{\mathrm{r}}} \right] \geq 1. \tag{10}$$

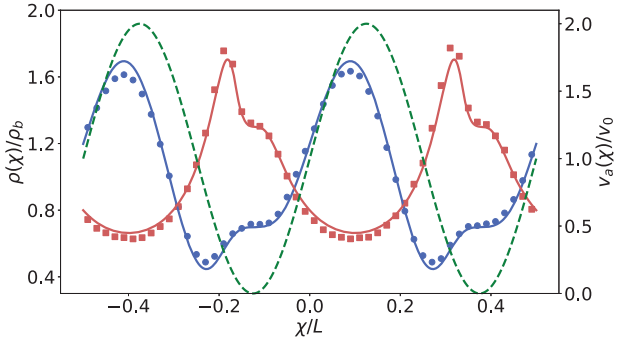


Fig. 2: Stationary density $\rho(\chi)$ of the dimer (red and blue lines and symbols, left axis), in the comoving frame of the traveling activity wave $v_{\rm a}(\chi)$ with sinusoidal shape (green dashed line, eq. (11), right axis), as obtained from numerical simulations (symbols) and from analytical predictions (eq. (12), solid lines). The latter hold under the assumption of long wavelength and slow traveling wave and they are reported for both a high-friction cargo with $q = q_{\rm high} > q_{\rm th}$ (blue) and a low-friction cargo with $q = q_{\rm low} < q_{\rm th}$ (red). See the section "Simulation details" for further information.

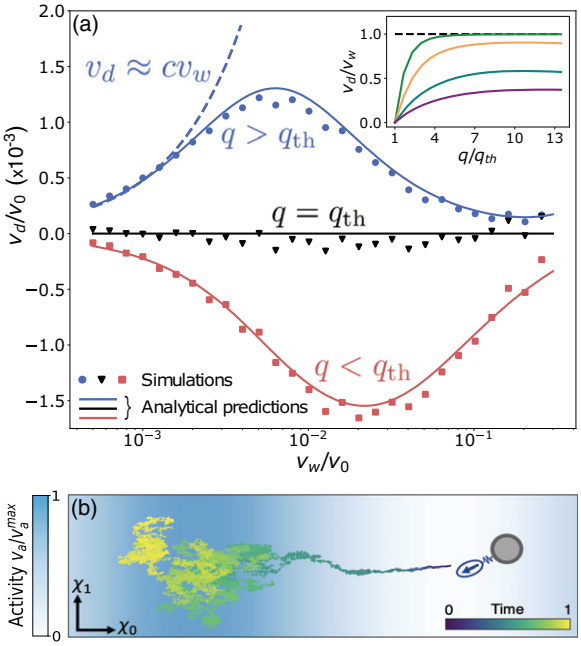


Fig. 3: (a) Average drift $v_d$ as a function of the phase velocity $v_w$ in the slow-wave regime $v_w < v_0$ (eq. (13)). For low-friction cargoes with $q = q_{\rm low} < q_{\rm th}$ (red line), the microswimmer exhibits a negative tactic behavior. At the threshold value $q_{\rm th}$ (black line), the average drift vanishes for all wave velocities $v_w$, whereas for $q = q_{\rm high} > q_{\rm th}$ (blue solid line), the dimer is characterized by positive taxis. Details on numerical results (symbols) can be found in section "Simulation details". In the inset, we report the slope of the linear relation $v_d \approx cv_w$ (blue dashed line) at small wave velocities as a function of $q$, and for thermal diffusivity $D \in \{0.05,\ 0.03,\ 0.01,\ 0.001\}$ (solid lines from bottom to top). (b) Stochastic trajectory of a cargo-carrying microswimmer in the comoving frame $(\chi_0, \chi_1)$ in two spatial dimensions. For a high-friction cargo ($q = 20$) and small thermal diffusivity $D = 10^{-3}$ the dimer "surfs" the propagating activity wave by localizing around its maximum while traveling with the same velocity, *i.e.*, $v_d = v_w$.

For highly mobile cargoes with $q < q_{\rm th}$ one has $\epsilon > 0$ and thus the dimer preferentially accumulates in low-activity regions. For slow cargoes with $q > q_{\rm th}$, instead, $\epsilon < 0$ and the dimer preferentially accumulates in high-activity regions. Interestingly, as in the single-particle case (see, *e.g.*, ref. [40]), the equivalence with a cargo-carrying ABP [32] with rotational diffusivity $D_r$ is fully recovered by imposing $\tau^{-1} = (d-1)D_r$.

In order to analyze the general case of an activity travelling wave ($v_w \neq 0$), we assume for simplicity that the activity field $v_{\rm a}$ varies only along $\boldsymbol{e}_0$. Accordingly, we denote the effective drift and diffusivity with $D_{\rm eff}(\chi_0)$ and $V_{{\rm eff},\alpha}(\chi_0)$ as they now depend only on $\chi_0 = \boldsymbol{\chi}\cdot\boldsymbol{e}_0$. As an example, we hereafter consider a sinusoidal activity wave

$$v_{\rm a}(\chi_0) = v_0\,[1 + \sin(\chi_0/\lambda)], \tag{11}$$

with wavelength $\lambda$, but the derivation can be easily extended to activity traveling waves with different shapes. We determine the resulting stationary density $\rho(\boldsymbol{\chi})$ in the comoving frame

$$\frac{\rho(\boldsymbol{\chi})}{\rho_b} = \frac{L\,D_{\rm eff}^{-1}(\chi_0)\int_0^L {\rm d}x \exp\left\{-\int_{\chi_0}^{\chi_0+x} {\rm d}y \frac{V_{{\rm eff},0}(y)}{D_{\rm eff}(y)}\right\}}{\int_0^L {\rm d}u \int_0^L {\rm d}x\, D_{\rm eff}^{-1}(u) \exp\left\{-\int_u^{u+x} {\rm d}y \frac{V_{{\rm eff},0}(y)}{D_{\rm eff}(y)}\right\}}, \tag{12}$$

by considering a comoving box of size $L$ with periodic boundary conditions. Here, $\rho_b = L^{-d}$ is the value of the uniform distribution over the $d$-dimensional comoving box. The stationary density $\rho(\boldsymbol{\chi})$ is shown in fig. 2 and it also features the transition in the preferential accumulation illustrated above for $v_w = 0$. Moreover, the interaction with a propagating activity field induces a non-trivial tactic response in the microswimmer, which is now able to sustain a non-vanishing stationary flux $J_0$ in the comoving frame, acquiring an average drift velocity $v_d = (\langle\dot{\boldsymbol{r}}_1\rangle + q\langle\dot{\boldsymbol{r}}_2\rangle)/(1+q) = J_0/\rho_b + v_w$ along $\boldsymbol{e}_0$ in the lab frame. This drift is given by [41,42]

$$v_d = \frac{L\left[1 - \exp\left\{-\int_0^L {\rm d}y \frac{V_{{\rm eff},0}(y)}{D_{\rm eff}(y)}\right\}\right]}{\int_0^L {\rm d}u \int_0^L {\rm d}x\, D_{\rm eff}^{-1}(u) \exp\left\{-\int_u^{u+x} {\rm d}y \frac{V_{{\rm eff},0}(y)}{D_{\rm eff}(y)}\right\}} + v_w, \tag{13}$$

and it strongly depends on the tactic coupling $\epsilon$ and therefore on $q$. More precisely, it can be shown analytically that $v_d$ vanishes at the static threshold value $q = q_{\rm th}$ in eq. (10) (see sect. 3 of the SM). Additionally, for sufficiently small thermal diffusivity $D$, the threshold value $q = q_{\rm th}$ also separates two distinct tactic regimes with respect to the wave propagation: *positive taxis* for $q > q_{\rm th}$, where the microswimmer navigates along the propagating tactic signal with $v_d/v_w > 0$, and *negative taxis* for $q < q_{\rm th}$, where the microswimmer navigates against it, with $v_d/v_w < 0$, see fig. 3(a). This predicted negative taxis as well as the fact

that its magnitude decreases upon increasing $D$ are consistent with what occurs for a single active particle [25,26], which is retrieved as the limit $q \to 0$ of our model. Conversely, as $q$ increases, the response of the dimeric microswimmer to the traveling tactic signal might become substantially different from that of a single active particle, depending on both $q$ and $\tau/\tau_{\rm r}$. More precisely, at fixed $\tau/\tau_{\rm r}$ the cargo-carrying microswimmer travels along the sinusoidal wave when $q > q_{\rm th}$, due to its tendency to localize close to the propagating activity crests, performing the *active surfing* shown in fig. 3(b). Interestingly, an analogous effect was observed experimentally with single self-polarizing phototactic particles in traveling light pulses [24]. While in ref. [24] this behavior is caused by an aligning torque, in our model it emerges as a cooperative effect between the active carrier and the passive cargo. Note, however, that the ability of the microswimmer to catch up with the travelling wave crests, *i.e.*, $v_d \simeq v_w$ is limited to the case of slowly propagating activity wave, which explains the non-monotonicity of the blue curve in fig. 3(a). In order to quantify the efficiency of this surfing, we determine the slope $c$ of the linear relation $v_d \approx c v_w$, which holds at small wave velocities $v_w$. Its dependence on $q$ and the thermal diffusivity $D$ is reported in the inset of fig. 3, which shows, as expected, that $c \leq 1$ and that the directed transport is highly efficient (*i.e.*, $c \simeq 1$) for $D \ll \tau v_0^2$.

We recall here that the predictions presented above follow from a coarse graining which assumes that the activity field varies slowly on a length scale of the order of $l_p = v_0\tau$. In the static case $v_w = 0$, this condition is met for $\lambda \gg l_p$. However, for a traveling wave, the coarse graining additionally requires that the distance $\sim v_w\tau$ traveled by the active wave on a time scale $\sim \tau$ does not exceed $\sim l_p$, which happens for $v_w < v_0$. Accordingly, in order to investigate the transport properties in the opposite case $v_w > v_0$, we pursue below an alternative analytical approach.

**Transport properties for fast activity waves.** – For simplicity, and without loss of generality, we restrict the analysis of the case $v_w > v_0$ to one-dimensional systems and to a sinusoidal traveling wave as in eq. (11). The main difference compared to the slow-wave approximation discussed above lies in the closure scheme used to combine the mode eqs. (3) and (4). More precisely, as the small gradients approximation is no longer applicable for $v_w > v_0$, we explore this regime by considering small self-propulsion forces by keeping in the effective dynamics only contributions of the lowest order in $v_0$ [29,43,44]. To this aim, we rewrite eq. (4) in the more convenient form

$$\hat{\mathcal{L}}_\sigma \sigma(\chi, r, t) = -\frac{\partial_\chi \left[v_{\rm a}(\chi')\varphi\right]}{(1+q)} - \partial_r \left[v_{\rm a}(\chi')\varphi\right] + \Upsilon(\chi, r, t), \tag{14}$$

where $\chi' = \chi + qr/(1+q)$ is the position of the active carrier in the comoving frame, $\Upsilon(\chi, r, t)$ includes all contributions of higher-order modes, and the operator $\hat{\mathcal{L}}_\sigma$ is defined as

$$\hat{\mathcal{L}}_\sigma = \partial_t + \frac{1}{\tau} - v_w\partial_\chi - \frac{D}{1+q}\partial_\chi^2 - \frac{(1+q)D}{q}\left[\partial_r^2 + \frac{1}{\ell^2}\partial_r r\right], \tag{15}$$

with the characteristic length $\ell = \sqrt{D\tau_{\rm r}}$.

To solve for $\sigma(\chi, r, t)$, we then determine the Green function of $\hat{\mathcal{L}}_\sigma$ and compute the convolution with the r.h.s. of eq. (14). In doing this, we assume that the contribution $\Upsilon(\chi, r, t)$ of higher-order modes is negligible in the limit of small self-propulsion forces, thus closing the hierarchy. Analogously to the previous approach, after integrating over the relative coordinate $r$, we obtain a continuity equation for the marginal density $\rho(\chi, t)$, *i.e.*,

$$\partial_t \rho(\chi, t) = -\partial_\chi \left[I(\chi, t) - \frac{D}{1+q}\partial_\chi \rho - v_w \rho\right], \tag{16}$$

where

$$I(\chi, t) = \int_{-\infty}^{\infty} {\rm d}r\, \frac{v_{\rm a}(\chi')\, \sigma(\chi, r, t)}{(1+q)} = \frac{\langle v_{\rm a}(\chi')\eta \,|\, \chi\rangle}{1+q}\rho(\chi, t), \tag{17}$$

and $\langle\cdot|\chi\rangle$ denotes the conditional average at fixed $\chi$. We derive a close yet cumbersome analytical expression for $I(\chi, t)$ which is related to the local average swim speed of the center of friction due to self-propulsion, see eq. (17) and sect. 4 of the SM). Similarly, we also derive in the SM analytical expressions for the stationary density and the flux in the comoving frame, which we use to analyze the directed transport in the regime of fast active traveling waves. In particular, for $D\tau_{\rm r} \ll \lambda^2$, the average drift velocity $v_d$ reads

$$\frac{v_d}{v_0} = \frac{l_p}{2\lambda(1+q)^2}\left[\frac{\sin\psi_0}{|z_0|} + q\frac{\sin\psi_1}{|z_1|}\right], \tag{18}$$

where we recall that $l_p = v_0\tau$ is the persistence length of the microswimmer, while $\psi_n$ and $|z_n|$ are the phase and the modulus, respectively, of the complex number

$$z_n = 1 + \frac{\tau D}{\lambda^2(1+q)} + \frac{(1+q)\tau D}{q\ell^2}n + {\rm i}\frac{\tau v_w}{\lambda}, \tag{19}$$

where i is the imaginary unit. A general expression of the drift velocity for an arbitrary thermal diffusivity is given in sect. 4 of the SM.

Figure 4 shows the behavior of the average drift $v_d$ as a function of the wave velocity $v_w$ in the regime $v_w > v_0$ of fast traveling waves. Unlike the case of $v_w < v_0$ (see fig. 3), the tactic behavior of the microswimmer does not exhibit a qualitative change as a function of the friction ratio $q$, with the drift occurring always along the direction of the active wave. However, as $q$ increases, this drift decreases because of the reduced mobility of the dimer. The drift velocity of the microswimmer attains its maximum value at a wave speed which scales as $v_w/v_0 \sim \lambda/l_p$. This can be qualitatively understood as follows. Consider a single pulse of activity of spatial extent $\lambda$ travelling with a speed

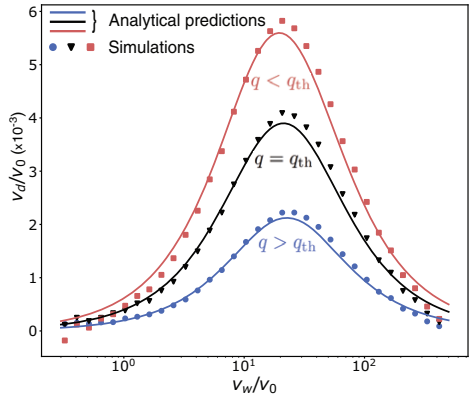


Fig. 4: Average drift velocity $v_d$ as a function of the phase velocity $v_w$ of the activity wave for $v_w > v_0$ (eq. (18)). The cargo-carrying microswimmer acquires a positive drift independently of the value of the friction ratio $q$. The numerical results (symbols) were obtained as discussed in the section "Simulation details".

$v_w$. A microswimmer with its polarization against the direction of the travelling pulse will rapidly exit the pulse from the receding front. However, when the polarization is along the direction of the pulse, the microswimmer will be carried along with it until it switches its polarization which will cause it to exit the pulse. The optimum scenario corresponds to the condition $v_w\tau - v_0\tau \sim \lambda$ in which the microswimmer effectively traverses the whole pulse before switching polarization. This results in a maximum of the drift speed at $v_w \sim \lambda/\tau$.

While the drift velocity of the dimer in fig. 4 features a single peak, we find both analytically and via numerical simulations that a second peak may appear at larger $v_w$, for large values of $q$ and persistence time $\tau$. The location of this additional peak depends on the spring relaxation time scale $\tau_{\rm r}$ but we defer a thorough investigation of its features and microscopic origin to future works.

**Simulation details.** – All numerical data have been obtained from Langevin dynamics simulations of the discretized version of eqs. (1), using the Euler-Maruyama scheme with integration timestep $\Delta t = 0.01$. In particular, the density in fig. 2 has been numerically estimated on a time series coming from a single simulation of duration $10^8$ steps, using periodic boundary conditions with a cell size of $L = 10$. Other simulation parameters were: $v_w = 10^{-2}$, $v_0 = 1.0$, $\tau = 0.1$, $\kappa = 5$, $\gamma = 1.0$, $D = 10^{-3}$ (note that $k_BT = \gamma D = 10^{-3}$), $\lambda = 10/(4\pi)$, $q_{\rm high} = 4$ and $q_{\rm low} = 1$. The numerical results in figs. 3 and 4 were obtained by computing $(\chi(t) + v_w t - \chi(0))/t$ for each of $N = 10^3$ independent stochastic trajectories of length $t = 10^6\Delta t$ with open boundary conditions, and averaging such a quantity over different realizations. In this case we used $D = 10^{-2}$.

**Discussion.** – Our work shows that self-propelled cargo-carrying microswimmers interacting with a traveling wave of activity display a rich tactic behavior. Their response to such a wave is actually independent of the details of the activity, as evidenced by the proved equivalence of cargo-carrying AOUPs and ABPs in terms of their coarse grained dynamics. The tactic transition which emerges in the presence of slowly propagating waves relies on the possibility to control the preferential accumulation of the microswimmer in high/low activity regions, by tuning the friction of its cargo. In particular, we find a surfing effect when the directed migration along the activity wave is induced by an effective localization around the wave maxima. Considering, *e.g.*, the experimental realization of Janus microswimmers as in ref. [24], eq. (10) implies $q_{\rm th} \simeq \kappa/(0.02\,{\rm pN}/\mu{\rm m})$ for $q_{\rm th} \gtrsim 1$. Accordingly, assuming for the cargo-carrier binding an elastic constant $\kappa \simeq 0.1\,{\rm pN}/\mu{\rm m}$, typical for soft matter, the tactic transition is predicted to occur at a cargo radius $\simeq 8\,\mu{\rm m}$, which is within experimental reach. By tuning the stiffness $\kappa$ of the spring between the active carrier and the passive cargo, one can shift the transition. A possible experimental system could be envisaged in which the linker between carrier and cargo is composed of colloidal chains. Recently, colloidal chains have been produced experimentally with tremendous control on length and stiffness, mimicking the behavior of flexible and semiflexible polymers [45,46]. We speculate that a qualitatively similar tactic behavior may emerge spontaneously in a binary mixture of mutually attractive active and passive particles, upon formation of clusters of different sizes. It has been recently shown that also molecules composed of two rigidly connected active particles [47] and dimers made of two active chiral particles [48] exhibit a transition in their effective localization in high/low activity regions. It will be interesting to study such active-matter systems subject to active traveling waves, and in the presence of external potentials [49,50].

We expect our predictions to have an impact on experimental studies on soft matter, biophysics, and nanotechnology. Important examples include cases in which synthetic Janus particles [51] and bacteria [52] have been used to efficiently transport and deliver microscopic objects in specific target sites. Moreover, our investigation could inspire future optimal design of existing *biohybrid* micromachines such as spermbots formed by assembling syntetic materials with sperm cells [53,54]. The taxis transition unveiled by our minimal stochastic model may also have implications in biological processes at the microscale in which traveling waves play a key role, *e.g.*, sound transduction in the cochlea [55,56] and signaling waves in cell development [57].

*Data availability statement*: The data that support the findings of this study are available upon reasonable request from the authors.

REFERENCES

[1] Jülicher F., Ajdari A. and Prost J., *Rev. Mod. Phys.*, **69** (1997) 1269.

[2] Hänggi P. and Marchesoni F., *Rev. Mod. Phys.*, **81** (2009) 387.
[3] Marchetti M. C., Joanny J.-F., Ramaswamy S., Liverpool T. B., Prost J., Rao M. and Simha R. A., *Rev. Mod. Phys.*, **85** (2013) 1143.
[4] Bechinger C., Di Leonardo R., Löwen H., Reichhardt C., Volpe G. and Volpe G., *Rev. Mod. Phys.*, **88** (2016) 045006.
[5] Fenteany G. and Glogauer M., *Curr. Opin. Hematol.*, **11** (2004) 15.
[6] Kanai Y., Dohmae N. and Hirokawa N., *Neuron*, **43** (2004) 513.
[7] Berg H. C., *E. coli in Motion* (Springer) 2004.
[8] Friedrich B. M. and Jülicher F., *Proc. Natl. Acad. Sci. U.S.A.*, **104** (2007) 13256.
[9] Mano T., Delfau J.-B., Iwasawa J. and Sano M., *Proc. Natl. Acad. Sci. U.S.A.*, **114** (2017) E2580.
[10] Reinišová L., Hermanová S. and Pumera M., *Nanoscale*, **11** (2019) 6519.
[11] Ebbens S., *Curr. Opin. Colloid. Interface Sci.*, **21** (2016) 14.
[12] García M., Orozco J., Guix M., Gao W., Sattayasamitsathit S., Escarpa A., Merkoçi A. and Wang J., *Nanoscale*, **5** (2013) 1325.
[13] Sánchez S., Soler L. and Katuri J., *Angew. Chem. Int. Ed.*, **54** (2015) 1414.
[14] Singh A. V., Hosseinidoust Z., Park B.-W., Yasa O. and Sitti M., *ACS Nano*, **11** (2017) 9759.
[15] Alapan Y., Yasa O., Schauer O., Giltinan J., Tabak A. F., Sourjik V. and Sitti M., *Sci. Robot.*, **3** (2018) 4423.
[16] Vaccari L., Molaei M., Leheny R. L. and Stebe K. J., *Soft Matter*, **14** (2018) 5643.
[17] Sentürk O. I., Schauer O., Chen F., Sourjik V. and Wegner S. V., *Adv. Healthc. Mater.*, **9** (2020) 1900956.
[18] Fisher P. R., Merkl R. and Gerisch G., *J. Cell. Biol.*, **108** (1989) 973.
[19] Martiel J.-L. and Goldbeter A., *Biophys. J.*, **52** (1987) 807.
[20] Tomchik K. J. and Devreotes P. N., *Science*, **212** (1981) 443.
[21] Goldstein R. E., *Phys. Rev. Lett.*, **77** (1996) 775.
[22] Gregor T., Fujimoto K., Masaki N. and Sawai S., *Science*, **328** (2010) 1021.
[23] Höfer T., Maini P., Sherratt J., Chaplain M., Chauvet P., Metevier D., Montes P. and Murray J., *Appl. Math. Lett.*, **7** (1994) 1.
[24] Lozano C. and Bechinger C., *Nat. Commun.*, **10** (2019) 2495.
[25] Geiseler A., Hänggi P., Marchesoni F., Mulhern C. and Savel'ev S., *Phys. Rev. E*, **94** (2016) 012613.
[26] Geiseler A., Hänggi P. and Marchesoni F., *Sci. Rep.*, **7** (2017) 41884.
[27] Geiseler A., *Artificial Microswimmers in Spatio-Temporally Modulated Activating Media*, PhD Thesis, University of Augsburg (2017).
[28] Sharma A. and Brader J. M., *Phys. Rev. E*, **96** (2017) 032604.
[29] Merlitz H., Vuijk H. D., Brader J., Sharma A. and Sommer J.-U., *J. Chem. Phys.*, **148** (2018) 194116.
[30] Popescu M. N., Tasinkevych M. and Dietrich S., *EPL*, **95** (2011) 28004.
[31] Baraban L., Tasinkevich M., Popescu M. N., Sanchez S., Dietrich S. and Schmidt O., *Soft Matter*, **8** (2012) 48.
[32] Vuijk H. D., Merlitz H., Lang M., Sharma A. and Sommer J.-U., *Phys. Rev. Lett.*, **126** (2021) 208102.
[33] Caprini L., Hernández-García E., López C. and Marini Bettolo Marconi U., *Sci. Rep.*, **9** (2019) 1.
[34] Martin D., O'Byrne J., Cates M. E., Fodor É., Nardini C., Tailleur J. and van Wijland F., *Phys. Rev. E*, **103** (2021) 032607.
[35] Caprini L., Sprenger A. R., Löwen H. and Wittmann R., *J. Chem. Phys.*, **156** (2022) 071102.
[36] Gopal A., Roldán E. and Ruffo S., *J. Phys. A*, **54** (2021) 164001.
[37] Cates M. E. and Tailleur J., *EPL*, **101** (2013) 20010.
[38] Solon A. P., Cates M. E. and Tailleur J., *Eur. Phys. J. ST*, **224** (2015) 1231.
[39] Adeleke-Larodo T., *Non-equilibrium dynamics of active enzymes*, PhD Thesis, University of Oxford (2020).
[40] Caprini L., Marconi U. M. B., Wittmann R. and Löwen H., *Soft Matter*, **18** (2022) 1412.
[41] Hänggi P., Talkner P. and Borkovec M., *Rev. Mod. Phys.*, **62** (1990) 251.
[42] Goel N. S. and Richter-Dyn N., *Stochastic Models in Biology* (Elsevier) 2016.
[43] Sharma A. and Brader J. M., *J. Chem. Phys.*, **145** (2016) 161101.
[44] Dal Cengio S., Levis D. and Pagonabarraga I., *Phys. Rev. Lett.*, **123** (2019) 238003.
[45] Vutukuri H. R., Demirörs A. F., Peng B., van Oostrum P. D. J., Imhof A. and van Blaaderen A., *Angew. Chem. Int. Ed.*, **51** (2012) 11249.
[46] Vutukuri H. R., Bet B., van Roij R., Dijkstra M. and Huck W. T. S., *Sci. Rep.*, **7** (2017) 16758.
[47] Vuijk H. D., Klempahn S., Merlitz H., Sommer J.-U. and Sharma A., *Phys. Rev. E*, **106** (2022) 014617.
[48] Muzzeddu P. L., Vuijk H. D., Löwen H., Sommer J.-U. and Sharma A., *J. Chem. Phys.*, **157** (2022) 134902.
[49] Caprini L., Marconi U. M. B., Puglisi A. and Vulpiani A., *J. Stat. Mech.*, **2019** (2019) 053203.
[50] García-Millán R. and Pruessner G., *J. Stat. Mech.*, **2021** (2021) 063203.
[51] Baraban L., Makarov D., Streubel R., Mönch I., Grimm D., Sanchez S. and Schmidt O. G., *ACS Nano*, **6** (2012) 3383.
[52] Akin D., Sturgis J., Ragheb K., Sherman D., Burkholder K., Robinson J. P., Bhunia A. K., Mohammed S. and Bashir R., *Nat. Nanotechnol.*, **2** (2007) 441.
[53] Medina-Sánchez M., Schwarz L., Meyer A. K., Hebenstreit F. and Schmidt O. G., *Nano Lett.*, **16** (2016) 555.
[54] Magdanz V., Medina-Sánchez M., Schwarz L., Xu H., Elgeti J. and Schmidt O. G., *Adv. Mater.*, **29** (2017) 1606301.
[55] Roberts W., Howard J. and Hudspeth A., *Annu. Rev. Cell. Biol.*, **4** (1988) 63.
[56] Duke T. and Jülicher F., *Phys. Rev. Lett.*, **90** (2003) 158101.
[57] Di Talia S. and Vergassola M., *Annu. Rev. Biophys.*, **51** (2022) 327.